International Journal of Nanomedicine

Dovepress

open access to scientific and medical research

Open Access Full Text Article

ORIGINAL RESEARCH

Dual-Modal Near-Infrared Organic Nanoparticles: Integrating Mild Hyperthermia Phototherapy with Fluorescence Imaging

Raluca Borlan[1,*], Madalina Tudor[1,2,*], Olga Soritau[3], Adrian Florea[4], Emoke Pall[5], Bogdan Pop[6,7], Dana Maniu[2], Simion Astilean[1,2], Monica Focsan[1,2]

[1]Nanobiophotonics and Laser Microspectroscopy Centre, Interdisciplinary Research Institute on Bio-Nano-Sciences, Babes-Bolyai University, Cluj-Napoca, Cluj, Romania; [2]Biomolecular Physics Department, Faculty of Physics, Babes-Bolyai University, Cluj-Napoca, Cluj, Romania; [3]Department of Radiobiology and Tumor Biology, Oncology Institute Prof. Dr. Ion Chiricuta, Cluj-Napoca, Cluj, Romania; [4]Department of Cell and Molecular Biology, Faculty of Medicine, Iuliu Hatieganu University of Medicine and Pharmacy, Cluj-Napoca, Cluj, Romania; [5]Department of Infectious Diseases, University of Agricultural Sciences and Veterinary Medicine, Cluj-Napoca, Cluj, Romania; [6]Department of Pathology, Oncology Institute Prof. Dr. Ion Chiricuta, Cluj-Napoca, Cluj, Romania; [7]Department of Pathology, University of Medicine and Pharmacy Iuliu Hatieganu, Cluj-Napoca, Cluj, Romania

*These authors contributed equally to this work

Correspondence: Monica Focsan, Biomolecular Physics Department, Faculty of Physics, Babes-Bolyai University; Nanobiophotonics and Laser Microspectroscopy Centre, Interdisciplinary Research Institute on Bio-Nano-Sciences, Str. Treboniu Laurian 42, Cluj-Napoca, 400271, Romania, Email monica.iosin@ubbcluj.ro

Purpose: Our study seeks to develop dual-modal organic-nanoagents for cancer therapy and real-time fluorescence imaging, followed by their pre-clinical evaluation on a murine model. Integrating NIR molecular imaging with nanotechnology, our aim is to improve outcomes for early-stage cutaneous melanoma by offering more effective and less invasive methods. This approach has the potential to enhance both photothermal therapy (PTT) and Sentinel Lymph Node Biopsy (SLNB) procedures for melanoma patients.

Methods: NIR-797-isothiocyanate was encapsulated in poly(D,L-lactide-co-glycolide) acid (PLGA) nanoparticles (NPs) using a two-step protocol, followed by thorough characterization, including assessing loading efficiency, fluorescence stability, and photothermal conversion. Biocompatibility and cellular uptake were tested in vitro on melanoma cells, while PTT assay, with real-time thermal monitoring, was performed in vivo on tumor-bearing mice under irradiation with an 808 nm laser. Finally, ex vivo fluorescence microscopy, histopathological assay, and TEM imaging were performed.

Results: Our PLGA NPs, with a diameter of 270 nm, negative charge, and 60% NIR-797 loading efficiency, demonstrated excellent stability and fluorescence properties, as well as efficient light-to-heat conversion. In vitro studies confirmed their biocompatibility and cellular internalization. In vivo experiments demonstrated their efficacy as photothermal agents, inducing mild hyperthermia with temperatures reaching up to 43.8 °C. Ex vivo microscopy of tumor tissue confirmed persistent NIR fluorescence and uniform distribution of the NPs. Histopathological and TEM assays revealed early apoptosis, immune cell response, ultrastructural damage, and intracellular material debris resulting from combined NP treatment and irradiation. Additionally, TEM analyses of irradiated zone margins showed attenuated cellular damage, highlighting the precision and effectiveness of our targeted treatment approach.

Conclusion: Specifically tailored for dual-modal NIR functionality, our NPs offer a novel approach in cancer PTT and real-time fluorescence monitoring, signaling a promising avenue toward clinical translation.

Keywords: organic nanoparticles, dual-modal agents, NIR fluorescence imaging, NIR phototherapeutic agents, mild hyperthermia, melanoma

Introduction

On a global scale, it is envisaged that the incidence of new cancer cases shall witness an impressive surge to approximately 47% by the year 2040. This projection primarily arises from population growth and the aging demographic, with potential aggravation stemming from the escalating prevalence of risk factors across various regions. Implementing primary prevention

Received: 9 April 2024
Accepted: 3 August 2024
Published: 5 September 2024

© 2024 Borlan et al. This work is published and licensed by Dove Medical Press Limited. The full terms of this license are available at https://www.dovepress.com/terms.php and incorporate the Creative Commons Attribution – Non Commercial (unported, v3.0) License (http://creativecommons.org/licenses/by-nc/3.0/). By accessing the work you hereby accept the Terms. Non-commercial uses of the work are permitted without any further permission from Dove Medical Press Limited, provided the work is properly attributed. For permission for commercial use of this work, please see paragraphs 4.2 and 5 of our Terms (https://www.dovepress.com/terms.php).

Graphical Abstract

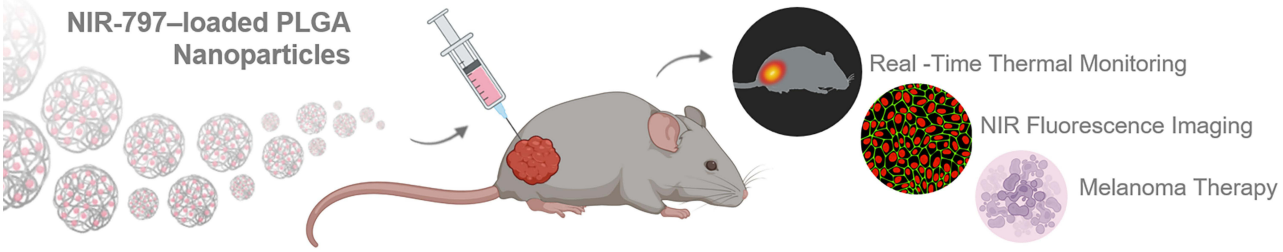

strategies emerges as a particularly effective approach in cancer control, given that approximately half of all cancer cases are preventable.[1] For instance, the mortality rate of melanoma, a deadly variant of skin cancer, has become a topic of paramount concern in recent years.

Melanoma prevention, consisting of minimizing exposure to known risk factors, such as ultraviolet radiation from sunlight or tanning beds, plays a crucial role in mitigating the burden of this aggressive form of skin cancer. In the bygone years, the melanoma death rate exhibited a disconcerting rise, accentuating the urgent need for enhanced awareness, prevention, and early detection strategies. However, over time, a glimmer of hope emerged as the melanoma mortality rate embarked on a gradual deceleration, indicating a progressive transition towards improved outcomes.[2] It is crucial to note, that despite these promising advancements, the 5-year survival rate for patients with metastatic melanoma remains below 30%.[3] Thus, melanoma persists as a formidable adversary, demanding continued vigilance and comprehensive strategies, due to its varied clinical presentations and the histologic similarities it shares with other tumor types. Clinical examination and biopsy are the primary diagnostic tools, but distinguishing between benign moles and melanoma can be difficult. Additional imaging and genetic testing are often needed for a more objective diagnosis. Moreover, early-stage melanoma patients with signs of metastasis or high-risk features should consider PET and MRI imaging, though guidelines vary for those with positive sentinel lymph nodes (SLN).[4]

The status of lymph nodes is a crucial prognostic factor in early-stage cutaneous melanoma, with 15 to 25% of patients exhibiting occult lymph node metastases despite having clinically unremarkable lymph nodes. Sentinel Lymph Node Biopsy (SLNB), is a minimally invasive procedure for nodal staging widely accepted in the management of melanoma.[5] Traditional SLNB uses radiocolloid based lymphoscintigraphy and blue dye, achieving a 96% SLN identification rate but posing radiation exposure and allergic reaction risks.[6]

To address the limitations associated with real-time monitoring and potential tissue injuries, researchers have explored the application of optical molecular imaging in SLNB. Optical molecular imaging holds significant promise in the life sciences due to its operational simplicity, noninvasiveness, high sensitivity, and cost-effectiveness.[7] Notably, fluorescence imaging enables real-time detection capabilities while ensuring an ample field of visualization, thereby enhancing its efficacy in intraoperative settings.[8] Fluorescence has become an essential technique for enhancing surgical visualization by clearly differentiating tissues from their surroundings. The absorption and emission of light by fluorophores significantly improve visibility compared to traditional white-light images. Therefore, the rapid expansion of fluorescence applications in medicine and surgery holds the potential to profoundly influence current practices.[9]

Fluorescence imaging employs a specialized camera to capture the emitted light from a fluorescent contrast agent, which is stimulated by an appropriate light source. This imaging technique can be seamlessly integrated into a compact open-field device or incorporated within laparoscopic or robotic instruments, enabling non-contact and real-time examination. By administering a fluorescent contrast agent,[10,11] the targeted organ or tissue can be visualized with remarkable sensitivity and contrasting properties. When it comes to medical applications, fluorescent agents emitting NIR wavelengths, ranging from 650 to 900 nm, offer distinct advantages. The skin exhibits an optical wavelength window characterized by minimal absorption coefficients of melanin, hemoglobin, and water, wherein melanin

demonstrates an absorption spectrum spanning 200–900 nm with variable peak absorption depending on its composition, predominantly in the ultraviolet range and gradually diminishing in the visible and infrared spectra, while hemoglobin exhibits peak absorption at blue (418 nm) and yellow/orange (542/577 nm) wavelengths. Ergo, NIR light, distinguished by its remarkable tissue penetration depth of several millimeters and diminished scattering compared to visible light, exhibits exceptional imaging properties, including minimal autofluorescence, thereby augmenting the quality and fidelity of the captured images.[12,13]

Furthermore, within the past 20 years, NIR light has found application in the field of therapy, particularly in the context of stimulating photothermal agents administered to the tumor site. These photothermal agents possess the capacity to absorb and transform incident light energy into thermal energy, thereby instigating localized hyperthermia, which leads to tumor inhibition or ablation through thermal-induced damage. Existing literature has extensively investigated the capacity of diverse photothermal agents to reach elevated localized temperatures, exceeding 50°C, during NIR laser irradiation, thereby initiating necrosis in cancerous cells.[14–20] Nevertheless, a limitation is encountered in the form of non-specific heat dispersion, resulting in unintended harm to adjacent healthy tissue, as well as the possibility of tumor recurrence due to immune evasion. To transcend these drawbacks, considerable efforts have been directed towards the implementation of PTT characterized by mild hyperthermia, which is defined as temperatures below 45°C, thus inducing direct cell death through protein denaturation.[21,22] More importantly mild hyperthermia can aid in the immune cell response activation as a secondary effect, thus opening new avenues for the synergistic functionality of PTT and immunotherapy for cancer treatment.[23] Given the superior tissue penetration of NIR fluorescence imaging and the efficacy of PTT via NIR irradiation, there is a strong clinical interest in dual-modal agents that can provide real-time tumor visualization and treatment, potentially revolutionizing patient care.

A diverse array of NPs formulations has been engineered to effectively encapsulate and transport dyes to specific cancer cell types, in order to surpass the deleterious adverse effects, limited photostability, and non-selective targeting associated with conventional free dye administration. The evident necessity of introducing a new generation of fluorescent agents, based on NIR dyes or novel alternatives loaded within nanostructures such as NPs, into clinical trials emerges to enhance tumoral drug internalization and achieve superior tumor-to-background ratios during surgical procedures. Notably, among the extensive repertoire of NPs currently undergoing clinical evaluation, with over 60 NPs approved by the Food and Drug Administration (FDA) for clinical trials, a substantial proportion of these NPs investigated in oncology studies fall within the realm of organic NPs.[24,25] For instance, the encapsulation of IR-817 in albumin NPs has been shown to enhance water solubility, reduce fluorescence quenching, and increase photothermal efficiency, leading to effective tumor ablation in melanoma models.[26] Additionally, novel methods for site-specific imaging and image-guided therapy, such as boron-dipyrromethene structures incorporating aza groups, combining NIR fluorescence with photoacoustic imaging, including its combination with photothermal therapy, have shown high photothermal conversion efficiency and photostability, finding them powerful in vivo tumor treatments.[27] Moreover, innovative silica-based core-shell NPs were developed,[28] which incorporate the organic photothermal agent polydopamine and the Bromodomain-Containing Protein 4 inhibitor JQ-1. By increasing the surface roughness of these NPs, their internalization and therapeutic effects were significantly improved. In animal studies, these NPs successfully eradicated melanoma, activated tumor-specific immune responses, and prevented metastasis and recurrence, demonstrating a promising strategy for combined cancer therapy. These advancements underscore the potential of organic NPs to revolutionize melanoma treatment through enhanced imaging and effective photothermal therapy.

PLGA, which stands for poly (lactide-co-glycolide acid), is a synthetic biodegradable polymer that was initially introduced in the 1960s as surgical sutures and monofilaments. However, its utility has expanded to encompass various polymeric biomaterial applications owing to its exceptional properties. PLGA has emerged as the most extensively investigated and widely employed polymer in controlled release systems, earning the status of being the gold standard for biodegradable polymers in the field of controlled release delivery platforms.[29] In contrast to natural polymers, synthetic polymers like PLGA possess the advantage of tailoring their chemical, physical, and mechanical properties, thereby exerting precise control over their degradation characteristics. Upon degradation, PLGA breaks down into harmless byproducts, namely carbon dioxide and water, which are eliminated through the Krebs cycle, posing no toxicological concerns.[30] PLGA is derived from the fermentation of lactic and glycolic acids obtained from sugars, endowing them

with environmentally friendly attributes. Regarding biomedical applications, the cytocompatibility of PLGA based NPs, loaded with Indocyanine Green, a FDA-approved NIR dye, was studied in vitro on prostate cancer cells by Patel et al.[31] The outstanding biocompatibility of PLGA and its capacity to degrade within the human body render it highly desirable for biomedical purposes having received approval from the FDA for intravenous, oral, and cutaneous administration in human subjects.[32]

In the contemporary clinical landscape, marked by a diligent endeavor to explore novel avenues for pertinent medical applications, the primary objective of our study resides in the development of cutting-edge organic dual-modal agents for a preliminary investigation into immediate pathological changes in cancer PTT and real-time fluorescence monitoring, followed by their pre-clinical evaluation on murine model. Moreover, our proposed agents are endowed with optical attributes situated within the NIR region of the electromagnetic spectrum, ensuring deeper tissue penetration for improved therapeutic and imaging outcomes. Precisely, the primary goals of the current study are to: i) fabricate PLGA NPs loaded with a NIR fluorophore (ie, NIR-797-isothiocyanate), further denoted as NIR-797–loaded PLGA NPs; ii) ensure optimal fluorescence properties; iii) utilize PTT to achieve targeted tumor mild hyperthermia and possibly activate an immune response against cancer cells; iv) maintain fluorescence after in vivo administration; v) determine the precision and effectiveness of the targeted therapy through histological and TEM analysis.

Materials and Methods

Materials

For this study we used the following materials: PLGA (lactide:glycolide – 50:50), NIR-797-isothiocyanate, poly (vinyl alcohol) PVA, Dulbecco′s Modified Eagle′s Medium (DMEM), Fetal Bovine Serum (FBS), L-glutamine, 4′,6-diamidino-2-phenylindole (DAPI) and Phalloidin–Tetramethylrhodamine B isothiocyanate (Phalloidin-TRITC) purchased from Sigma-Aldrich (Missouri, USA). Dimethyl sulfoxide (DMSO) and dichloromethane were purchased from CHEMPUR (Poland), and phosphate buffered saline (PBS) without calcium and magnesium was acquired from Lonza (Switzerland). We purchased $NaH_2PO_4 \cdot H_2O$, $Na_2HPO_4 \cdot 12H_2O$ from Reactivul (Romania), glutaraldehyde from Agar Scientific (UK); OsO_4, EMBED 812 from Electron Microscopy Sciences (Pennsylvania, USA); ethanol from VWR Chemicals (France), uranyl acetate from Merck (Darmstadt, Germany) and lead citrate from Fluka (Switzerland). The B16-F10 melanoma cell line was obtained from Prof. Zahan Marius at the University of Agricultural Sciences and Veterinary Medicine, Faculty of Zootechnics, but originally B16–F10 CRL-6475 ™ murine melanoma cell line was purchased from a certificated bank cell- ATCC (Manassas, VA, USA), and was approved by the Ethical Review Committee of the Oncological Institute "Prof. Dr. Ion Chiricuta". We obtained ultrapure water from the Milli-Q purification system - Millipore, Merck (Massachusetts, USA) that was used for all aqueous solutions.

Fabrication of NIR-797–Loaded PLGA NPs

For the fabrication of the PLGA NPs loaded with the commercially available fluorophore NIR-797, further denoted as NIR-797–loaded PLGA NPs, we adapted a two-step protocol from Patel et al.[31] The initial step entails the preparation of the NIR-797-isothiocyanate fluorophore in DMSO (1mg mL^{-1}), which was added dropwise to the PLGA solution. The latter was prepared employing 90 mg of PLGA and 3 mL of dichloromethane in an ice-cooled ultrasonic bath for a duration of one minute. Subsequently, the resulting mixture was left in the ice-cooled ultrasonic bath for a period of five minutes. The second step involves the precise syringe-based addition (using the NE-1000-Programmable Single Syringe Pump from New Era Pump Systems Inc., New York, USA, at a rate of 1mL min^{-1}) of the aforementioned solution into 12 mL of 5% PVA solution, while magnetically stirred, on a bed of ice. The final solution was maintained under continuous stirring at 200 rpm for an hour.

To purify the resulting particles, they were washed via centrifugation at 18000 rpm for 10 minutes to remove free NIR-797 molecules. The supernatant was discarded, and the remaining pellet was resuspended in PBS and centrifuged at 4000 rpm for 5 minutes to separate the NPs from any aggregates. The resulting supernatant, containing the NIR-797–loaded PLGA NPs, was collected.

Loading Efficiency and NIR-797 Payload in PLGA NPs

To quantify the NIR-797 dye captured within the newly fabricated PLGA NPs, we calculated the loading efficiency using the equation presented below (equation 1). NIR-797 was initially dispersed in DMSO (1mg mL^{-1}), followed by serial dilutions in 5% PVA solution. Subsequently, a calibration curve was established correlating varied NIR-797 concentrations (10^{-5}, $2x10^{-5}$, $3x10^{-5}$, $4x10^{-5}$, 5×10^{-5} M) with their corresponding optical densities measured at the peak absorption of NIR-797 in PVA solution, namely 684 nm. All measurements were performed in triplicate.

$$\text{Loading efficiency}(\%) = \frac{\text{Amount of NIR797 used} - \text{Amount of NIR797 present in supernatant}}{\text{Amount of NIR 797used}} \times 100 \quad (1)$$

As subsequent experiments called for a comparison between the behavior of the free dye and its encapsulated form, we took additional steps to determine more precisely the concentration of the NIR-797 fluorophore within the final NPs. Another calibration curve was established using various concentrations ($7x10^{-6}$, $8x10^{-6}$, $9x10^{-6}$, 10^{-5}, 2×10^{-5} M) of NIR-797 dispersed in PLGA solution, measured at 809 nm peak absorption. This allowed us to determine the concentration of the dye present in the aggregates, after removing them through centrifugation. The final payload of NIR-797 within the PLGA NPs was derived by subtracting the initial dye concentration used in the fabrication process from the concentrations found in both the supernatant and the pellet during the purification step.

Stability Analysis of NIR-797–Loaded PLGA Nanoparticles

To evaluate the temperature stability of NIR-797 both in free form and encapsulated within the NPs (24 μM concentration of NIR-797 was present in both samples), we measured their fluorescence emission during a process of controlled heating and cooling, with temperature increases in 5°C increments. The temporal stability of NIR-797–loaded PLGA NPs was evaluated by conducting dynamic light scattering (DLS) and zeta-potential measurements at one-week and one-month intervals during storage at 4°C in the dark.

Photothermal Effect

To validate the potential of NIR-797–loaded PLGA NPs as therapeutic agents, we studied their ability to convert light into heat. For this purpose, using a laser diode, 808 nm excitation wavelength, we irradiated 300 μL of NPs for 8 minutes until the maximum temperature stabilized. Thermal images were collected every 30 seconds during the 8-minute irradiation period and for another 15 minutes after the irradiation stopped, allowing the sample to cool down to room temperature, using an IR thermal imaging camera. Additionally, we examined the behavior of free NIR-797 dye in PBS, with the same concentration as the NPs (82 μM), for comparison. For control purposes, 300 μL of PBS solution and PLGA solution were irradiated as well. All measurements were performed in triplicate.

Next, we calculated the photothermal conversion efficiencies of free NIR-797 and NIR-797–loaded PLGA NPs based on the temperatures extracted from previously acquired thermal images. The calculations utilized the energy balance equation to assess the efficiency of light-to-heat conversion (equation 2).

$$\eta = \frac{h \cdot A \cdot \Delta T_{max} - I\xi}{I(1 - \xi)} \quad (2)$$

$$\xi = \frac{h \cdot A \cdot \Delta T_{max-H2O}}{I} \quad (3)$$

$$h\,A = \frac{\sum m_i C_{pi}}{\tau_s} \quad (4)$$

where h: heat transfer coefficient of the assayed material; A: area cross section of irradiation; ΔT_{max}: the difference between the maximum temperature and the initial temperature of the solution, I: irradiation power; ξ - the energy fraction absorbed by the cuvette and solvent; m_i: components masses; c_i: specific heats; τ_s: time constant describing the cooling process. The experimental values corresponding to these terms are summarized in Tables S2 and S3.

In vitro Assay

The B16-F10 melanoma cell line was employed for in vitro NIR-797–loaded PLGA NPs and free NIR-797 studies. The cells were maintained in DMEM medium (4.5 g l^{-1}), supplemented with FBS (10%), antibiotics (1%) and L-glutamine (2 mM), at 37°C in a humid incubator with 5% CO_2.

The toxicity of the free fluorophore as well as encapsulated in the newly fabricated polymeric NPs was evaluated via the MTT assay. Cytotoxicity refers to the ability of a substance to induce cell death. The MTT assay measures the metabolic activity of cells as an indicator of cell viability, proliferation, and cytotoxicity following treatment with the tested substance.[33] Melanoma cells were incubated in a 96-well microplate as follows: 10000 cells/well for 24-hour incubation experiments, 5000 cells/well for 48-hour incubation experiments, and 3000 cells/well for 72-hour incubation experiments. Different concentrations of the two solutions were added using serial dilutions, namely 1, 0.75, 0.62, 0.50, and 0.37 µM for the free dye, and 0.35, 0.7, 1.4, 2.8, and 5.6 µM for the dye encapsulated in PLGA NPs. Three wells were left untreated for each experiment as control samples. After 24 hours of incubation for the free dye, and 24, 48, and 72 hours for the NPs, the cells were washed, and the MTT colorimetric assay was performed. The percentage of cell viability for each concentration was calculated as the ratio of the sample absorbance to the control absorbance. All measurements were performed in triplicate.

For in vitro imaging, a total of 80000 B16-F10 cells were plated on 35 mm Ibidi µ-Dish dishes and incubated for 24 hours. Subsequently, the cells were treated with NIR-797–loaded PLGA NPs (final concentration of the dual-modal agent: 2.8 µM) to investigate the cellular uptake. After another 24 hours, the cells were rinsed thrice with PBS and fixed using a 4% paraformaldehyde solution. For nucleus highlighting, the cells were counterstained with an antifade medium containing 100 ng mL^{-1} DAPI, while Phalloidin-TRITC at a concentration of 50 µg mL^{-1} was employed to label the F-actin filaments.

In vivo Assay

B16-F10, a murine melanoma cell line originally derived from a spontaneous melanoma in C57BL/6 mice, was chosen for this study. The subcutaneous model, widely accepted for evaluating therapeutic strategies across various tumor models, was employed.[34] Our experimental design encompassed four distinct groups of mice, as follows. The positive control group consisted of mice exposed to irradiation and administered NIR-797–loaded PLGA NPs. Additionally, we examined three negative control groups: one without irradiation and lacking administration of NIR-797–loaded PLGA NPs, another subjected to irradiation but without the administration of the newly developed NPs, and a third group not exposed to irradiation but treated with NIR-797–loaded PLGA NPs.

Female C57BL/6 mice, aged 8–12 weeks and weighing 23.5 ± 0.5 g, were procured from the biobank at the Cluj-Napoca Oncological Institute. All animal maintenance and treatment procedures were conducted in strict adherence to the guidelines stipulated by the Host Institutional Animal Care, in accordance with both Directive No. 86/609/EEC and Directive No. 2010/63/EU. Ethical approval for the study was granted by the Ethical Review Committee of the Oncological Institute "Prof. Dr. Ion Chiricuta". The Ethics Committee of "Prof. I. Chiricuta" Oncological Institute Cluj-Napoca evaluated the study under file number 116/12.12.2018. Subcutaneous injections, including the inoculation of malignant cells, B16-F10 cell line, and the administration of NIR-797–loaded PLGA NPs, as well as PTT irradiation, were carried out following the intraperitoneal administration of anesthesia using a combination of ketamine (100 mg kg^{-1}) and xylazine (10 mg kg^{-1}). At the conclusion of the study, all mice were euthanized via cervical dislocation to facilitate sample collection.

To induce melanoma tumors, mice underwent shaving on the left flank, followed by subcutaneous injection of 5×10^5 B16-F10 cells suspended in 100 µL of physiological serum. Tumors developed to a size with a width of 7.5 ± 1.5 mm and a length of 13 ± 1.5 mm within 7 days, at which point treatment with NIR-797–loaded PLGA NPs commenced. This treatment involved the injection of 600 µL of the NPs suspension into both the peritumoral and intratumoral spaces. Peritumoral and intratumoral injections were chosen to maximize the accumulation of NPs in the tumor area, thereby enhancing photothermal efficiency and therapeutic effect. Four hours following the administration of NIR-797–loaded PLGA NPs, we initiated photothermal treatment of the tumors. The 4 hours period allows the NPs to accumulate sufficiently in the tumor,[35] reducing their presence in other tissues, thus enhancing the specificity and effectiveness of the

PTT treatment. During an 8-minute exposure to an 808 nm medical laser irradiation, we monitored the temperature variations on the tumor surface. The laser was positioned 3 cm away from the tumor, resulting in a calculated power density of 73.4 mW cm^{-2}. This monitoring was facilitated by the use of a thermal camera.

Ex vivo Assay

Tumors were harvested and processed 24 hours post-irradiation using various techniques. For fluorescence imaging, tumor tissue fragments were carefully embedded in OCT (optimal cutting temperature) medium and subsequently sectioned into 4 µm thick slices using a microtome cryostat.

Meanwhile, for classical histological analysis, the collected samples were fixed in a 10% formalin solution, followed by embedding in paraffin wax. These paraffin-embedded sections were then stained using the standard hematoxylin and eosin procedure for detailed histological examination.

Finally, to study the organelle ultrastructure, samples of less than 1 mm^3 removed from the excised tumors were processed for conventional TEM as follows: prefixation (minimum 2 h) with 2.7% glutaraldehyde in 0.1 M PBS (pH = 7.4); washed 4 times with PBS; postfixation (1.5 h) with 1% OsO4 in 0.15 M PBS (pH = 7.4); dehydration with an ethanol series (30–100% 30 min each) (until 70% ethanol all steps were performed at 2–4°C and the next ones at laboratory temperature); embedding in EMBED 812 epoxy resin, consecutive to resin infiltration with a series of resin-ethanol solutions. After cutting the polymerized blocks, ultrathin sections of 60–80 nm were collected on 300 mesh copper grids from Agar Scientific (UK), covered with formvar film, and contrasted 15 min with 13% uranyl acetate and 5 min with 2.8% lead citrate before imaging.

Equipment

The hydrodynamic diameter of NIR-797–loaded PLGA NPs was measured using DLS with a Zetasizer NanoZS90 instrument from Malvern Panalytical Ltd. (Worcestershire, UK) at 25°C. The measurements were performed in triplicate using disposable micro-cells (ZEN0040). The same instrument was utilized to determine their zeta-potential, employing disposable folded capillary cells (DTS1070), also in triplicate, at a temperature of 25°C.

To confirm the diameter of the newly fabricated NPs, we acquired images using a JEOL JEM 100CX II transmission electron microscope (TEM) from JEOL (Japan) equipped with a MegaView G3 camera from EMSIS (Germany). NIR-797–loaded PLGA NPs were dispersed onto carbon coated grids, and 0.5% uranyl acetate was added for negative staining. The voltage used for TEM imaging was set at 80 kV.

For the establishment of the calibration curves, the optical densities of the standard solutions were measured with the V-760 UV-Vis-NIR Spectrophotometer from Jasco International Co., Ltd. (Tokyo, Japan), using 2 mm quartz glass cuvettes from Hellma (Germany). Emission spectra were recorded at a fixed wavelength of 765 nm with a FP6500 spectrofluorometer from Jasco International Co., Ltd. (Tokyo, Japan), equipped with a Xenon lamp, using quartz glass cuvettes from Hellma (Germany). All measurements were performed at controlled temperature (25°C) using a Peltier thermostatting accessory. The fluorescence emission spectra were recorded from 785 to 890 nm, using different optical configurations, more precisely 5 nm, 10 nm bandpass slits for the experiments regarding the NPs and 3 nm, 10 nm bandpass slits for the free dye. All measurements were performed in triplicate.

To evaluate the photothermal capability of the dye in free form and encapsulated within the PLGA NPs we used a Therapy Laser DTL-BCD-01 from Apel Laser (Romania). This device is equipped with a laser probe SL1 featuring an 808 nm diode with a power output of 265 mW. Thermal images were collected using an IR camera with thermal vision, namely PI450 from Optris (Germany).

The cellular viability percentage for each concentration was calculated as the ratio between the sample's absorbance and the control's absorbance. The absorbance was recorded using a Synergy 2 microplate reader (BioTek, Vermont, USA). Statistical analysis of the MTT viability test data was conducted using GraphPad Prism Software (Version 9.0, La Jolla, USA). Two-way ANOVA multiple comparison test followed by Bonferroni posttest was applied, with statistical significance set at a p-value of <0.05. The internalization of NIR-797–loaded PLGA NPs within B16-F10 cell line was imaged at an inverted Zeiss LSM980 NIR confocal microscope using a C-Apochromat 40x/1.2 NA water objective. DAPI, Phalloidin-TRITC and NIR-797–loaded PLGA NPs were

imaged using a 405/561/730 nm laser with 0.2/0.09/0.4% laser power, 1.36 µs pixel dwell time, 700/700/720 V Detector Gain, and the detection windows 411–544/552-694/755-802 nm respectively. Images were acquired at 1.2x Nyquist sampling (106x106x12.9 µm, 1546×1546 pixels) and processed with a linear deconvolution (LSM plus/ZEN blue version 3.7).

To evaluate the photothermal capability of the PLGA NPs in vivo, we used the same Therapy Laser DTL-BCD-01 and the images were collected using a FLIR-one infrared thermographic camera from Teledyne FLIR (Oregon, United States). The ex vivo epifluorescence images of the collected tissue were acquired using a pE-100 770 nm LED from CoolLED (UK) and an ICG-B filter set (Ex 769/41, Em 832/37), with an ECLIPSE Ti2-E inverted microscope from Nikon (Japan), equipped with a CFI Plan Fluor 40×/0.75 N.A. Ph2 objective, on a CCD PCO EDGE 4.2 digital camera and were analysed with NIS Elements software (version 5.11.02).

TEM imaging was used to analyse the organelle ultrastructure of excised tumors. The polymerized blocks were cut with a MT18212 DIATOME diamond knife from Hatfield (Pennsylvania, USA) on a Bromma 8800 ULTRATOME III ultramicrotome from LKB (Sweden) and examined with the same JEOL JEM 100CX II transmission electron microscope.

For processing, analysing, and visualizing the collected data, the following software was used: OriginPro 9.0 from OriginLab Corporation and GraphPad Prism 6 from GraphPad Software Inc.

Results and Discussion

Characterization of NIR-797–Loaded PLGA NPs

Considering medical applications, the intravenous administration of substances like drugs, contrast agents, or NPs is governed by size considerations. The goal is to extend circulation time, reduce renal excretion, and avoid entrapment by the reticuloendothelial system. Thus, our research focuses on the fabrication of PLGA NPs, loaded with NIR-797 fluorophore through a two-step protocol (Figure 1a), envisioned as dual-functional photothermal and contrast agents for medical diagnosis and therapy. Our NIR-797–loaded PLGA NPs, as measured by DLS, resulted in an average hydrodynamic diameter of 271 ± 4 nm with an average polydispersity index (PDI) of 0.2 ± 0.1 (Figure S1a). This aligns with the associated particle size histogram (over 400 NPs assessed), which was obtained via TEM imaging (Figure 1b), indicating a size of 238 ± 4 nm (Figure 1c). The zeta-potential measurements (Figure S1b) serve as an initial indicator of the NPs stability, with an average value of −66 ± 6 mV. Consequently, our newly developed dual-modal agents, with diameters in the optimal size range and negatively charged surfaces, are designed to ensure passive accumulation at tumor sites via the enhanced permeability and retention (EPR) effect,[36] promoting sustained retention within cancerous tissue.

To determine the loading efficiency of the fluorescent dye within the polymeric NPs, we constructed a calibration curve (Figure S2a) using different concentrations of free NIR-797 in PVA solution. We utilized an equation derived from Patel et al [31] for our calculations, and we adapted and optimized our fabrication method based on this work. The average loading efficiency achieved using our method was 60.0 ± 1.5%, surpassing the value reported in the aforementioned paper (48.8 ± 5.5%) where Indocyanine Green was encapsulated within the PLGA NPs. Since the subsequent experiments necessitate a comparative analysis of the free dye's behavior versus its encapsulated state, we employed an alternative method to accurately determine the payload of NIR-797 fluorophore within the NPs. To accomplish this, we established another calibration curve using various concentrations of NIR-797 in PLGA solution (Figure S2b). The resulting concentration served as the basis for subsequent experiments and comparative analyses.

Further evidence confirming the successful formation of NIR-797-loaded PLGA NPs is observed through a 9 nm shift in the maximum absorption peak, specific to monomers, of the dye loaded within the NPs compared to that of the free NIR-797, as depicted in Figure S3a, along with a 3 nm shift in the maximum emission peak (NPs: 809 nm, free NIR-797: 806 nm), as shown in Figure S3b.

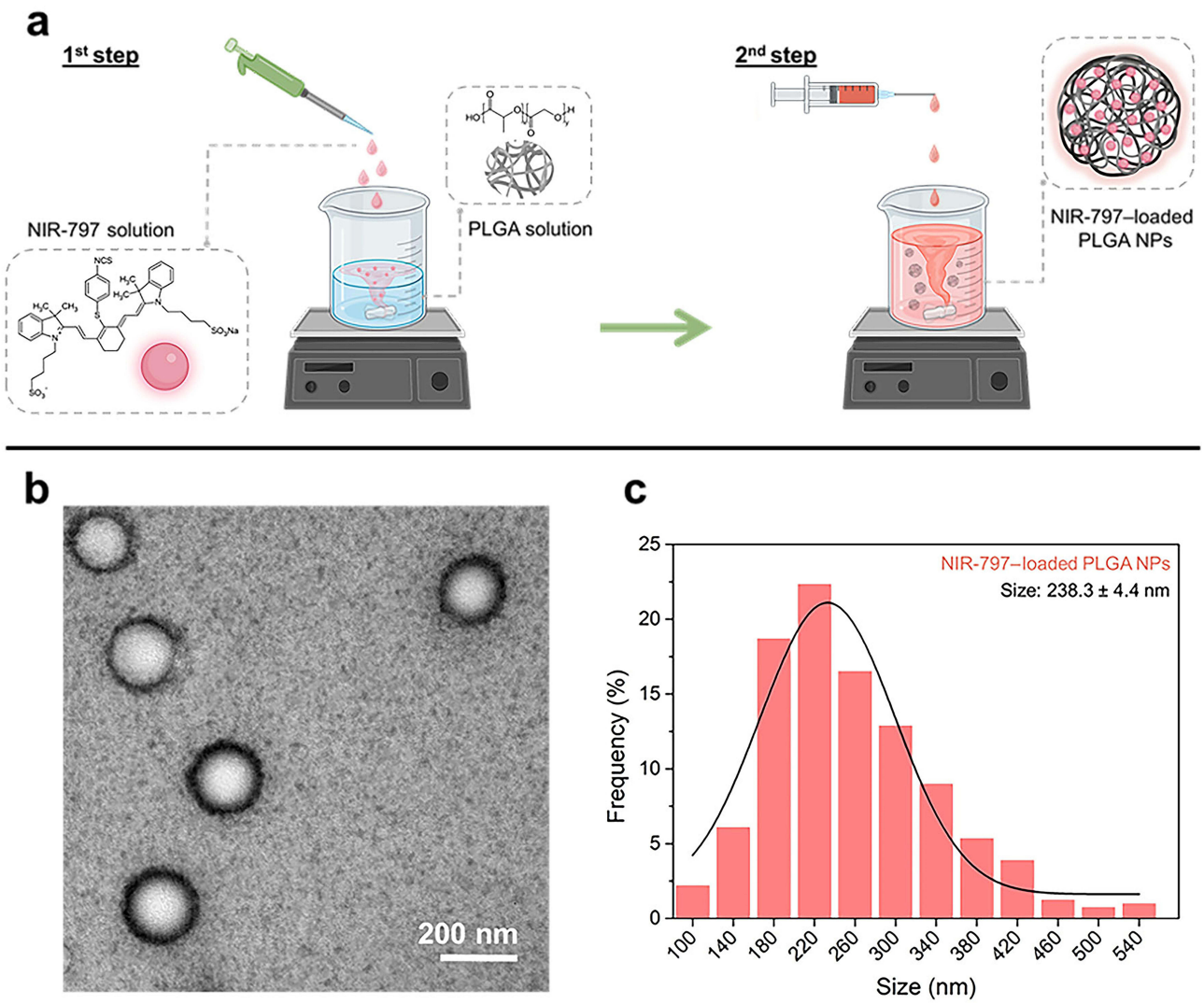

Figure 1 (**a**) Illustration of the adapted two-step fabrication protocol for NIR-797–loaded PLGA NPs. Created with BioRender.com (**b**) TEM image of NIR-797–loaded PLGA NPs. (**c**) NPs' size histogram.

Assessing Stability Factors in NIR-797–Loaded PLGA NPs

Thermal Effect on Fluorescence

One crucial consideration for biomaterials intended for medical applications is their response to thermal interactions. Consequently, we examined the fluorescence emission behavior of NIR-797, both in its free form and when encapsulated within PLGA NPs, as the temperature was gradually raised to biologically relevant levels ranging from 25 to 45°C. Figure 2a illustrates the linear correlation between emission intensity growth and increasing temperature for the free dye, with the process being reversible.

Similarly, Figure 2b demonstrates the same behavior for the NPs, although with a more pronounced increase in fluorescence intensity as the temperature rises. The fluorescence intensity of the free NIR-797 increases by up to 20%, whereas the intensity of the nanoparticle-encapsulated dye can reach as high as 45%, when compared to fluorescence intensity measurements taken at room temperature (Figure 2c). Intriguingly, the increase in fluorescence intensity of the free NIR-797 dye could be explained by the molecular structure of the dye itself. It is widely known that the family of cyanine dyes tend to form aggregates in solution;[37] thus, by increasing the temperature and providing thermal energy to the system, it can overcome the intermolecular forces holding the aggregates together. As the aggregates dissociate into monomers or smaller oligomers, the available non-radiative pathways for the decay of the excited state may be reduced,

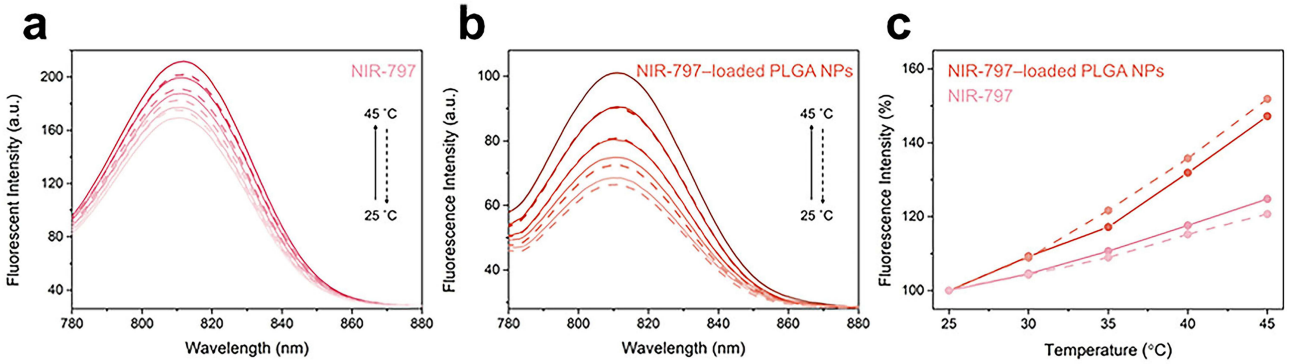

Figure 2 Measurements of fluorescence emission spectra of (**a**) Free NIR-797 solution and (**b**) NIR-797–loaded PLGA NPs at selected temperatures during heating (solid line) and cooling (dashed line) cycles. 24 μM concentration of NIR-797 was present in both samples. (**c**) Changes in the fluorescence emission intensity quantified as percentages – to note that the intensity at 25°C was considered as 100% in both cases.

leading to an increase in fluorescence. Moreover, some cyanine dyes may have flexible structures that can adopt different conformations in aggregated versus monomeric states. Temperature-induced changes could lead to conformational changes that favor monomeric forms, which are typically more fluorescent. On the other hand, the rise in intensity of the NIR-797–loaded PLGA NPs may also be explained by the particular orientation of the fluorophore within the NPs matrix that allows for energy transfer between dye molecules, leading to quenching. Temperature changes could disrupt these orientations, decreasing energy transfer and increasing the fluorescence emission. However, the fluorescence emission increase of the NIR-797–loaded PLGA NPs can also be attributed to the chemical interplay between the NIR-797 molecules and the PLGA matrix. As temperature rises, the matrix of the NPs may become more flexible; this increased flexibility could reduce the quenching interactions between the NIR-797 molecules and the matrix, thus allowing for higher fluorescence efficiency.

It is noteworthy that both free NIR-797 and NIR-797–loaded PLGA NPs exhibit no shift in the emission maximum during the heating and cooling process, indicating their remarkable temperature stability. This information highlights the potential of NIR-797–loaded PLGA NPs for biomedical applications, as their fluorescence properties remain reliable under physiological conditions.

Fluorescence Stability and Photobleaching

Photobleaching stability is a fundamental factor in medical imaging, influencing imaging quality, diagnostic precision, and therapeutic monitoring. This characteristic ensures a more consistent and reliable signal, contributing to improved diagnostic accuracy. It also allows for accurate diagnoses by preventing misinterpretations due to signal loss and minimizes the risk of false negatives. In therapeutics, photostability allows long-term monitoring of fluorescently labelled cells or drugs, providing insights into their distribution and effectiveness. Moreover, in fluorescence-guided surgery, photobleaching-resistant agents aid in the accurate identification and removal of cancerous tissues. Given these considerations, the development of NIR-797–loaded PLGA NPs, able to retain 86% (Figure S4) of their fluorescence after 30 minutes of excitation exposure, represents a significant achievement. Exhibiting high photostability, these NPs are poised to not only meet the rigorous demands of medical imaging but also contribute to advancements in diagnostics and therapeutics.

Temporal Trends: DLS and Zeta-Potential

The temporal stability of NIR-797–loaded PLGA NPs, regarding their size and surface charge, was assessed through DLS and zeta-potential measurements. These measurements were initially taken immediately after NPs fabrication (T0), with follow-up measurements performed after one week and one month of storage. Table S1 summarizes the obtained results, indicating minimal and insignificant variations in the hydrodynamic diameter and PDI of the NPs. Additionally, the zeta-potential values maintained within a range indicative of stability, further corroborating the sustained stability of the NIR-797–loaded PLGA NPs over time.

Photothermal Efficiency Assessment

The assessment of the light-to-heat conversion performance of PLGA NPs loaded with NIR-797 was conducted through the acquisition of thermal images after an 8-minute exposure to 808 nm laser irradiation, followed by a 15-minute cooling period to return to room temperature. The evaluation included a comparative analysis with free NIR-797 and control samples consisting of PLGA solution and PBS, employing the same experimental protocol. Figure 3a illustrates that the temperature of the NIR-797–loaded PLGA NPs increases rapidly, reaching a maximum rise of 9°C, to a peak temperature of 34°C within the first 6 minutes of irradiation. The observed increase in temperature falls within the optical range, making it sufficiently high to induce cell death without causing damage to the surrounding tissue. In contrast, the temperature of the free NIR-797 dye exhibits a time-dependent escalation, reaching a maximum increase of 17°C (maximum reached temperature of 42°C) within 8 minutes of irradiation. Under identical experimental conditions, negligible temperature variations were observed for the control samples. Next, utilizing the data extracted from the photothermal images, we generated thermal curves (Figure 3b) and determined the photothermal conversion efficiencies of the studied samples (Tables S2 and S3), leveraging theoretical models cited in the literature.[38] The results revealed a reduced efficiency for the encapsulated dye within the polymeric NPs (30.5 ± 0.2% for NIR-797–loaded PLGA NPs) compared to the free NIR-797 solution (43.7 ± 0.6%). In addition, the photothermal stability of the NPs was assessed through two successive cycles of heating and cooling (Figure S5). In the second cycle the NPs exhibited a maximum temperature rise of 3°C, while the free fluorophore showed a maximum rise of 11°C, indicating thermal losses. This disparity can be attributed to two main factors: i) within the nanoparticle matrix, the rotation or vibration of the NIR-797 molecules may be inhibited, mechanisms that typically aid in the dissipation of absorbed light energy as heat; ii) due to the scattering effect of the PLGA NPs, the intensity of light that the encapsulated NIR-797 molecules can absorb is diminished, thus the energy available for conversion into heat is reduced. Nonetheless, the light-to-heat conversion efficiency of our NPs is noticeably superior to that of Indocyanine Green (3.1%[39]), which is among the limited number of FDA-approved substances with NIR optical properties for medical applications. This comparison underscores the considerable potential of our NPs as effective photothermal agents in medical settings.

In vitro Studies

Cell Viability

The initial stride in the in vitro characterization of the freshly fabricated NIR-797–loaded PLGA NPs is represented by the assessment of cellular viability using the MTT assay on the B16-F10 melanoma cell line. We first investigated the potential cytotoxic effects from the free NIR-797 fluorophore, and as shown in Figure 4a, the dye exhibits concentration-dependent toxicity with an IC50 value of 0.19 µM. Subsequently, we performed viability tests on cells treated with the fluorophore encapsulated within the polymeric NPs, using three different incubation periods: 24, 48 and 72h. Figure 4b

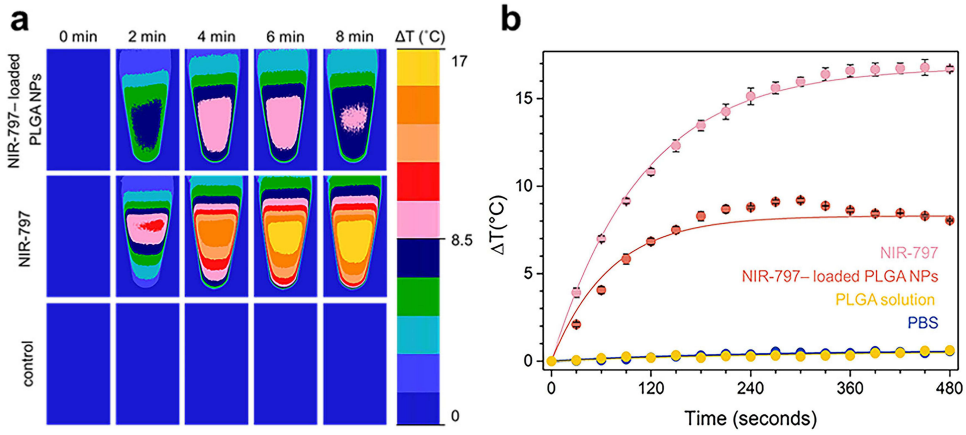

Figure 3 (**a**) Thermal images of NIR-797–loaded PLGA NPs, free NIR-797 solution, and control solution at the initial time and 2, 4, 6 and 8 min during irradiation with an 808 nm laser diode. (**b**) Thermal curves over an 8 min irradiation period, showing the response with respect to time for free NIR-797 solution (pink), NIR-797–loaded PLGA NPs (Orange), and PLGA solution (yellow) and PBS (blue) as control. NIR-797 concentration of 82 µM was present in both samples.

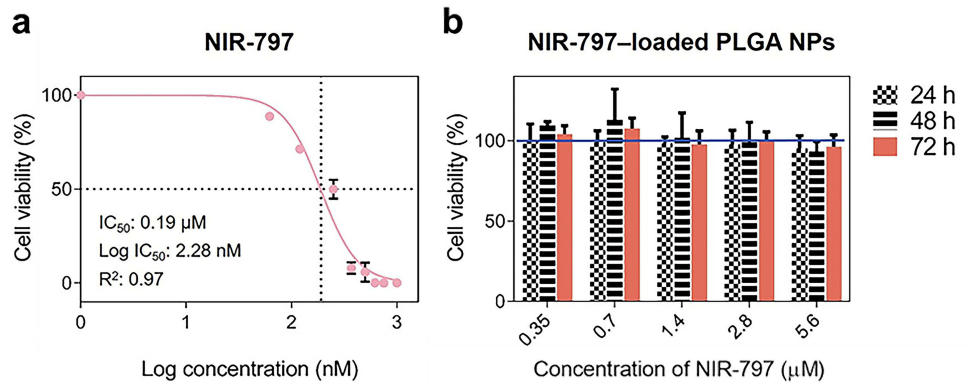

Figure 4 (**a**) Survival curve of melanoma cells treated with free NIR-797 dye. (**b**) MTT assay performed on melanoma cells treated with NIR-797–loaded PLGA NPs incubated at three different time periods. Control group is represented by the blue horizontal line.

reveals that melanoma cells incubated with concentrations below 1 µM of the NIR-797–loaded PLGA NPs solution showed minimal proliferation. The statistical analysis of the MTT viability test data, performed using Two-way ANOVA followed by the Bonferroni posttest, indicates that there are no statistically significant differences between the samples treated with various concentrations of NIR-797 loaded PLGA NPs and the controls at 24 hours, 48 hours, and 72 hours after testing (Table S4, Figure S6). Furthermore, no cytotoxic effects of the NPs were observed, even at concentrations approximately 30 times higher (5.6 µM) than the IC50 value of the free fluorophore. This highlights the biological compatibility of our NIR-797–loaded PLGA NPs, positioning them as promising candidates for potential dual-modal agents in the field of medicine.

Fluorescence Imaging

Employing confocal fluorescence microscopy images (Figure 5), we investigated the cellular localization of NIR-797–loaded PLGA NPs within melanoma cells after 24 hours of incubation. For clear visualization of NPs distribution, we

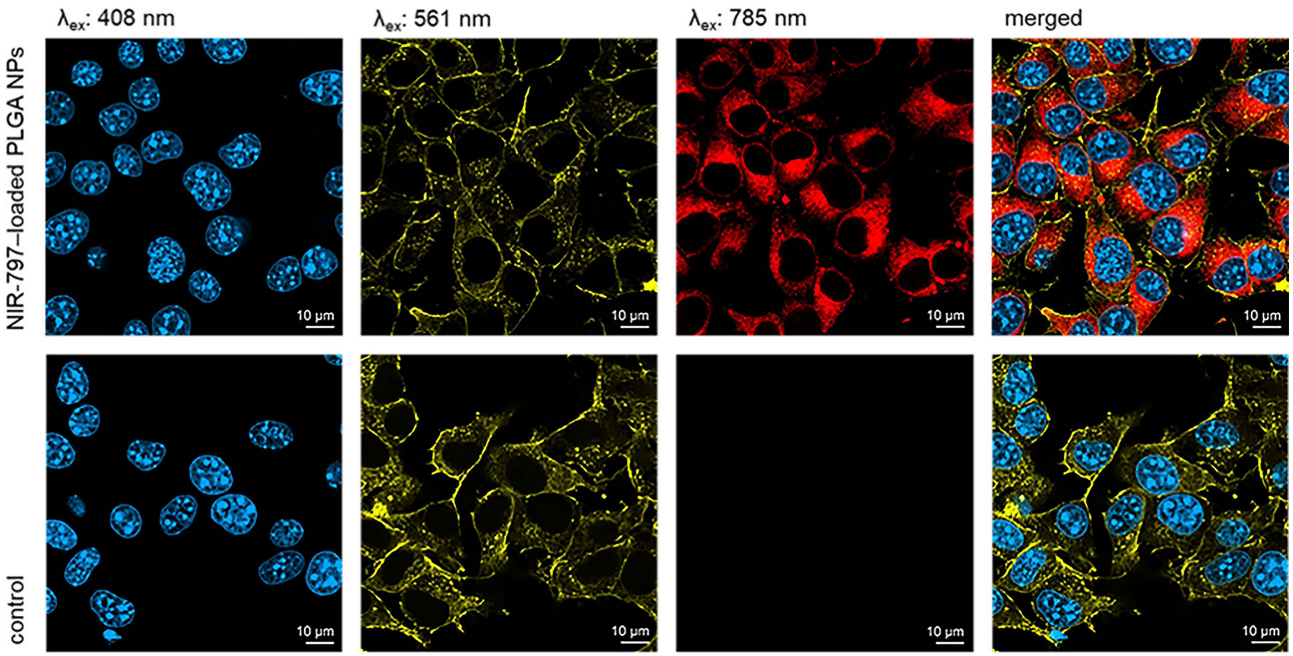

Figure 5 Fluorescence images of B16-F10 melanoma cells treated with NIR-797–loaded PLGA NPs (top) and control group (bottom). The cells were stained with DAPI and Phalloidin-TRITC.

labelled the nucleus with DAPI (blue) and the F-actin filaments, a component of the cytoskeleton, with Phalloidin-TRITC (yellow).

The top row presents images of cells treated with NIR-797–loaded PLGA NPs, while the bottom row shows images of untreated cells serving as the control sample. For the specific visualization of different cellular structures and the NPs in the cells, three lasers were used sequentially to excite the nucleus, the F-actin filaments, and the NPs, with wavelengths of 408, 561 and 785 nm, respectively. The last image in each row represents the overlay of the aforementioned fluorescence images, providing a clear representation of the localization and distribution of the NPs within the cells, as well as a comparison with the untreated control cells. Thus, Figure 5 reveals a uniform distribution of NIR-797–loaded PLGA NPs (red) throughout the cellular body, while no penetration into the nucleus is observed. These results affirm the excellent uptake of the newly fabricated NPs by melanoma cells, further validating their biocompatibility and potential as fluorescent contrast agents for tumor detection.

In vivo Studies

To assess the light-to-heat conversion performance of our newly developed NPs, we monitored the photothermal process in murine models 4 hours post-administration of the NIR-797–loaded PLGA NPs, following the changes in temperature during an 8-minute exposure to 808 nm medical laser (namely the positive control group). As illustrated in Figure 6, the surface temperature of the tumor rises gradually, reaching a maximum of 43.8°C in 8 minutes, consequently inducing mild hyperthermia. In addition, three negative control groups were examined: one without irradiation and lacking administration of NIR-797–loaded PLGA NPs, another exposed to irradiation but without administration of the newly developed NPs, and a third group without irradiation but treated with NIR-797–loaded PLGA NPs. The irradiated negative control group presents a slight increase in temperature (Figure S7), similar to the one Xiao et al [40] reported in their work on HeLa tumor-bearing mice. In the aforementioned paper, NIR-797 molecules underwent self-assembly within NPs and encountered subsequent modification with C18PMH-PEG5000. However, as a result of this encapsulation and modification, the temperature achieved upon 10-minute irradiation with an 808 nm laser reached 62°C, exceeding the upper limit of mild hyperthermia.

Ex vivo Studies

Fluorescence Imaging

Succeeding the in vivo trials, tissue samples from the melanoma tumors were inspected using epifluorescence imaging to determine whether the NIR-797–loaded PLGA NPs' fluorescent signal persisted. As shown in Figure 7, the probes collected from the mice treated with our NPs (positive control and negative control without irradiation but treated with the NPs groups) exhibit significant fluorescence intensity, indicating a uniform distribution of the NIR-797–loaded PLGA NPs within the entire tumor tissue. In contrast, the negative control groups without NPs administration displayed no fluorescence activity (Figure S8). In addition, liver tissue was collected for subsequent analysis. Figure S9 provides evidence that the NIR-797–loaded PLGA NPs enter the circulatory system following intra- and peritumoral administration, as their presence is detected in the liver. This study constitutes the preliminary evidence that our developed NIR-797–loaded PLGA NPs demonstrate effectiveness as fluorescent contrast agents and may be implemented in the near future in clinical use.

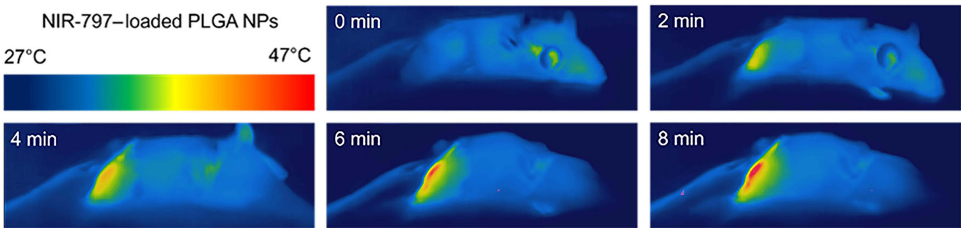

Figure 6 Thermal images of a melanoma-bearing mouse after 4 hours peri-tumoral and intra-tumoral injection with NIR-797–loaded PLGA NPs, following irradiation with an 808 nm laser diode for 8 minutes.

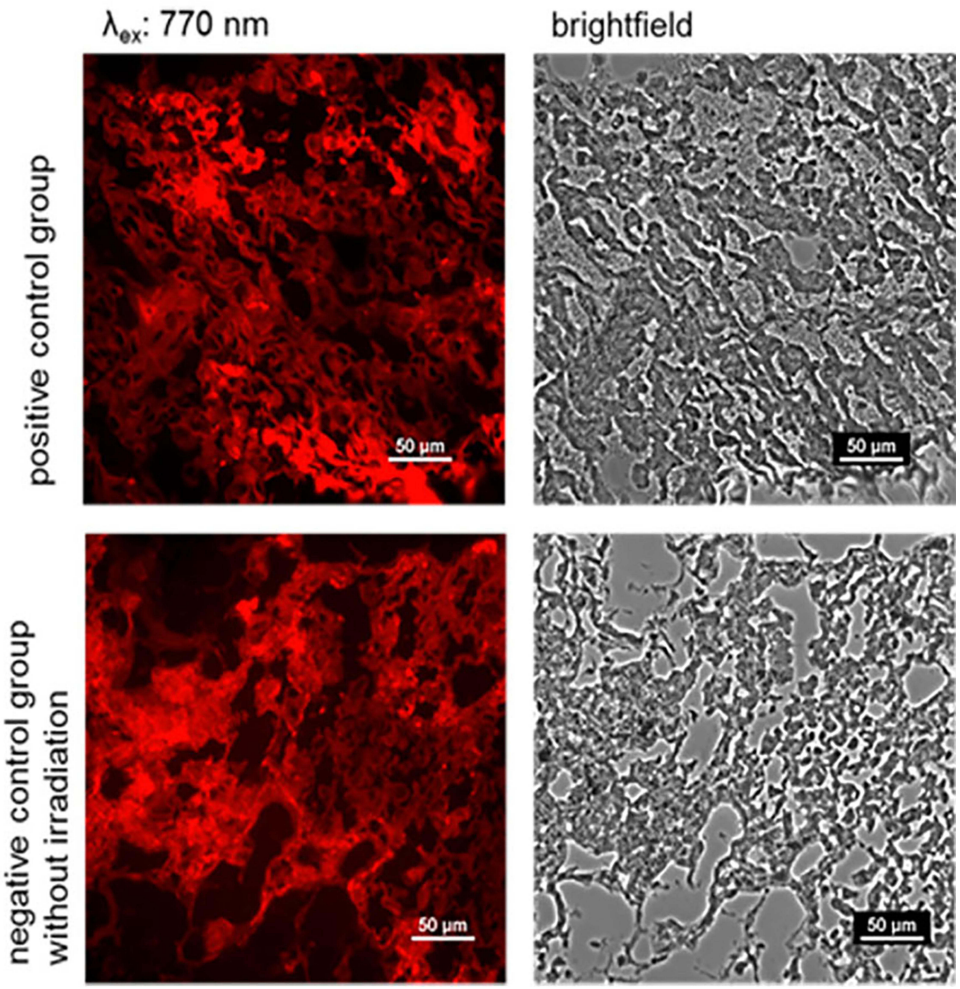

Figure 7 Ex vivo fluorescence and brightfield images of samples collected from tumorous tissue of positive control group (top) and negative control group (bottom) without irradiation.

Histopathological Findings

Histological examination encompassed a comprehensive analysis of various morphological aspects within the tumors, including necrosis, angiogenesis, and tumor burden. In our experimental model, characterized by tumor growth without neoangiogenesis involvement, we observed varying degrees of necrosis in all samples. Signs of tumor necrosis, such as nuclear fading and the appearance of disorganized cellular regions with more eosinophilic areas, were evident.[41] Notably, the positive control group exhibited early apoptosis, microhemorrhages, and an increased presence of infiltrated monocytes and macrophages (Figure 8a,e). This heightened immune response underscores the potential advantages of combined treatment with NIR-797–loaded PLGA NPs and NIR irradiation. In the negative control group, without irradiation and lacking administration of NIR-797–loaded PLGA NPs, we detected necrotic regions (approximately 5% of the total area) in the central portion of the melanoma tumors, along with characteristic tumor plaques with no signs of angiogenic features, such as tumor vessels (Figure 8b,f). The irradiated negative control group showed a higher level of necrosis (around 30% of the tumor volume), along with microhemorrhages, indications of cell apoptosis at the tumor margins, few fibroblasts, and infiltrated polymorphonuclear cells (Figure 8c,g). In the negative control group, without irradiation but treated with NIR-797–loaded PLGA NPs, (Figure 8d,h), distinct changes were observed. These changes included the presence of apoptotic areas accompanied by microhemorrhages, cellular edema, and an increased infiltration of immune cells, including monocytes, macrophages (likely melanophages), and polymorphonuclear cells. Additionally, this sample exhibited a reduced incidence of necrotic regions (~5%). We identified melanophages, characterized as round cells without nuclei or with faded nuclei, in

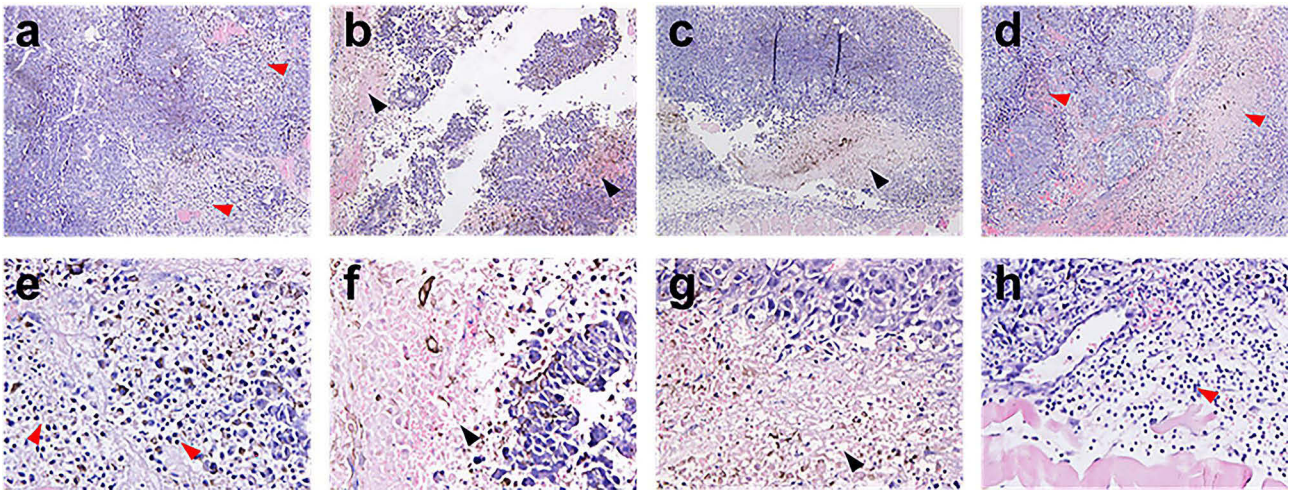

Figure 8 Histological aspects of Hematoxylin & Eosin staining of subcutaneous induced mice melanoma: (**a**) Positive control group; (**b**) Negative control group, without irradiation and lacking administration of NIR-797–loaded PLGA NPs; (**c**) Irradiated negative control group; (**d**) Negative control group without irradiation but treated with NIR-797–loaded PLGA; (**e**) Positive control group; (**f**) Negative control group, without irradiation and lacking administration of NIR-797–loaded PLGA NPs; (**g**) Irradiated negative control group; (**h**) Negative control group without irradiation but treated with NIR-797–loaded PLGA. The top row images correspond to a magnification of 10x, whereas the bottom row images to a magnification of 40x. Black arrow indicates regions of necrosis and red arrow indicates regions with immune cells infiltrations and apoptotic cells.

contrast to melanocytes containing melanin deposits.[42] The presence of infiltrated macrophages with phagocytic activity indicates their role in adaptive immunity, by presenting antigens to T cells and recruitment of lymphocytes and potential contributions to the host's response to the tumor microenvironment.[43] Immune cell infiltration within melanoma tumors treated with our NIR-797–loaded PLGA NPs, with or without irradiation, can be attributed to the host's immune response which, in the context of melanoma, such infiltration is considered a favorable prognostic indicator. Existing literature further supports the correlation between a moderate to marked presence of intratumoral and/or peritumoral lymphocytes in primary melanoma and improved patient survival outcomes.[44,45] Histological analysis prominently underscored the pronounced early apoptosis, increased immune cell infiltration and microhemorrhages observed in the positive control group. This robust immune response, particularly in the context of melanoma, a mechanism probably induced as a consequent of mild hyperthermia,[23] emphasizes the potential benefits of combined treatment with NIR-797–loaded PLGA NPs and NIR irradiation.

TEM Imaging

In order to acquire information regarding the effects of PTT on the cellular structure, TEM images of melanoma tumors samples were analysed. Figure 9 depicts the repercussions of the melanoma-bearing mice treated with NIR-797–loaded PLGA NPs after the 8-minute irradiation with an 808 nm medical laser (positive control group). A first indication of ultrastructural cellular damage is represented by the elongation of the mitochondria (Figure 9a), triggered by the endoplasmic reticulum (ER) stress-induced autophagy, as a protective mechanism.[46,47] Moreover, cytoplasmic vacuolization and the expansion of the ER alongside the presence of autophagosomes in the studied cells suggest cellular death (Figure 9b–d).[48] To our best knowledge, TEM images of PLGA NPs within cells or tissues are currently lacking in literature due to the inherent challenges in distinguishing them from other cellular components of similar density. However, it remains possible that the PLGA NPs (* notation in Figure 9d) are located within secondary lysosomes, appearing as spheres with reduced density and similar diameters, as to the dry size of PLGA NPs observed previously in Figure 1b. Furthermore, the necrotic demise of melanoma cells was substantiated by the final two images (Figure 9e and f), depicting cellular degradation highlighted by the debris of intracellular materials and the extravasation of red blood cells, also observed in the histological results discussed previously. Moreover, by collecting imaging samples from the borderline of the irradiated zones, we observed a less severe cell reaction, indicating the ability of our method to perform targeted therapy. In the negative control group

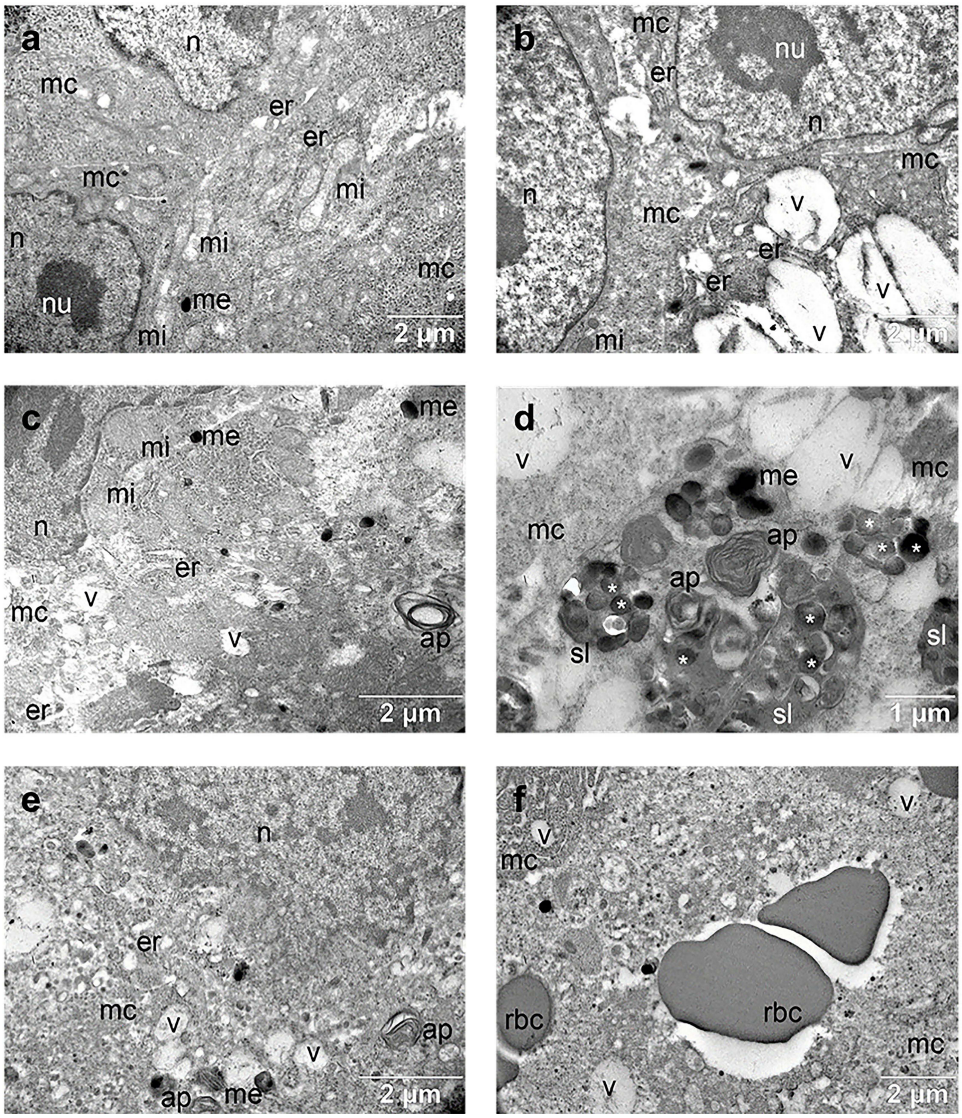

Figure 9 Ex vivo TEM images of positive control group: (**a**) elongated mitochondria; (**b**) cytoplasmic vacuolization and expanded ER; (**c**) extended cytoplasmic vacuolization and autophagosomes; (**d**) autophagosomes, melanosomes, vacuoles, elongated mitochondria, secondary lysosomes; (**e**) autophagosomes, melanosomes, vacuoles; (**f**) debris of a necrotic melanoma cell mixed with blood cells outside capillaries.

Note: * – NIR-797–loaded PLGA NPs.

Abbreviations: n, nucleus; nu, nucleolus; er, endoplasmic reticulum; me, melanosomes; rbc, red blood cell; mc, melanoma cell; mi, mitochondria; v, vacuoles; ap, autophagosome; sl, secondary lysosomes.

and the one treated with NPs without irradiation, as depicted in Figure 10a and b, respectively Figure 10e and f, the melanoma cells appeared compact with normal mitochondrial and ER ultrastructure. More precisely, in Figure 10b,f, blood capillaries are outlined, delineated by endothelial cells with normal aspect, indicating the integrity of the blood vessel structure. However, in Figure 10c and d, representing the irradiated negative control group, cytoplasmic vacuolization, elongated mitochondria, and dilated ER confirmed cellular degradation, being in accordance with histological analysis, thus possibly resulting from tumor expansion.

The notable outcomes demonstrating cell death induction and targeted therapeutic effects represent pivotal milestones in substantiating the potential utility of our NIR-797–loaded PLGA NPs, in combination with NIR irradiation, as efficacious photothermal agents. These findings hold considerable promise for their prospective application in clinical settings, thereby underscoring their significance in advancing therapeutic modalities.

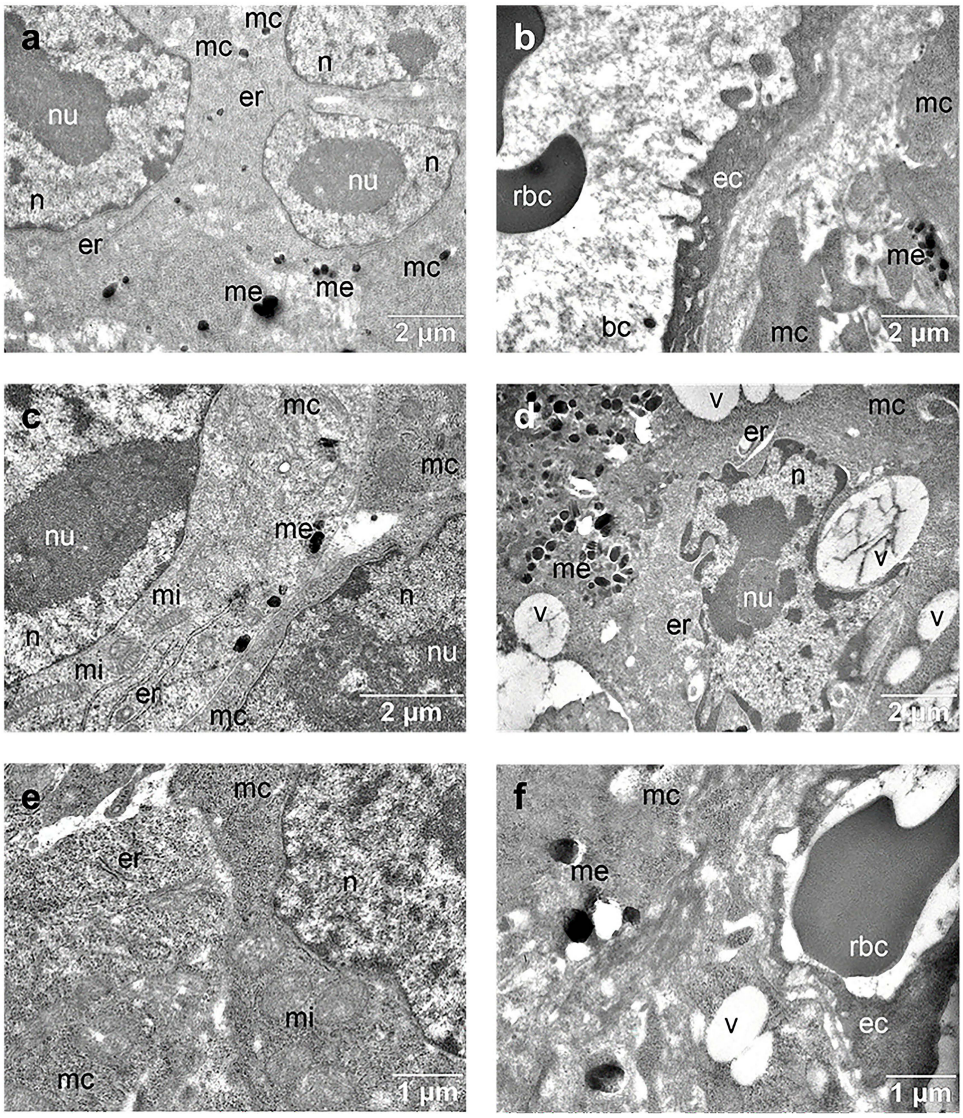

Figure 10 Ex vivo TEM images of negative control groups: (**a** and **b**) negative control group without irradiation and lacking administration of NIR-797–loaded PLGA NPs; (**c** and **d**) negative control group exposed to irradiation but without NPs administration; (**e** and **f**) negative control group without irradiation but treated with NIR-797–loaded PLGA NPs.
Abbreviations: n, nucleus; nu, nucleolus; er, endoplasmic reticulum; me, melanosomes; rbc, red blood cell; ec, endothelial cell; bc, blood capillary; mc, melanoma cell; mi, mitochondria; v, vacuoles.

Conclusion

Our study seeks to engineer a novel generation of NIR dual-modal agents aimed at addressing the pressing need for more effective and less invasive methods in cancer therapy and imaging, particularly for early-stage cutaneous melanoma and SLNB procedures. We successfully achieved this goal by developing NIR-797–loaded PLGA NPs and demonstrating their multifaceted utility through a series of comprehensive characterizations, including in solution studies, in vitro assay on melanoma cells, as well as in vivo and ex vivo evaluation on a murine melanoma model.

We employed a meticulous two-step protocol to encapsulate NIR-797 within PLGA NPs. Notably, our newly developed NPs exhibited a diameter of approximately 240 nm, being in the optimal range for biomedical applications, negative surface charge, and an impressive loading efficiency of 60% for NIR-797. In addition, NIR-797–loaded PLGA NPs showed remarkable stability in solution, maintaining their structural integrity and fluorescence properties even under biologically relevant temperatures, with a mere 15% decrease in fluorescence intensity observed over a 30-minute exposure to excitation light.

In vitro studies established the biocompatibility of the NIR-797–loaded PLGA NPs, ensuring their suitability for biomedical applications. This assurance arises from the encapsulation of the NIR-797 fluorophore within the PLGA NPs, which not only guarantees safe delivery but also capitalizes on the biocompatibility of the organic polymer PLGA, thus reducing the risk of adverse reactions. Confocal fluorescence microscopy confirmed the successful internalization of NPs by B16-F10 melanoma cells, further highlighting their potential for targeted delivery and imaging.

In vivo PTT studies on melanoma tumor-bearing mice demonstrated the ability of the NPs to effectively convert light into heat using an 808 nm laser, resulting in mild hyperthermia conducive to targeted cell death. Real-time thermal monitoring was achieved to modulate the temperature increase to a safe range, thus mitigating the risk of off-target effects.

Ex vivo fluorescence imaging of tumor tissue revealed the persistent presence and uniform distribution of NPs, indicating their potential as fluorescent contrast agents for image-guided surgical resection. Histological and TEM analyses provided further insights into the therapeutic mechanisms and effects of our dual-modal NPs. We observed early apoptosis, immune cell infiltration, and ultrastructural changes indicative of cell death mechanisms, affirming the targeted therapeutic effects of our approach. Moreover, TEM images of irradiated zone margins suggested attenuated cellular damage, highlighting the precision and effectiveness of our targeted treatment strategy.

These findings collectively demonstrate the robust effectiveness and multifaceted utility of our engineered NIR-797–loaded PLGA NPs in both cancer therapy and real-time imaging. Furthermore, the triggered immune response could offer synergistic benefits if combined with immunotherapy in future studies.

In summary, our engineered NIR-797–loaded PLGA NPs have demonstrated robust effectiveness as both photothermal and fluorescent contrast agents, meeting our initial objectives. The findings not only lay a solid groundwork for future research but also represent a significant advance in the development of dual-modal tools for targeted cancer treatments, opening avenues for broader biomedical applications.

Abbreviations

DAPI, 4′,6-diamidino-2-phenylindole; DLS, dynamic light scattering; DMEM, Dulbecco's Modified Eagle's Medium; DMSO, Dimethyl sulfoxide; EPR, enhanced permeability and retention; ER, endoplasmic reticulum; FBS, Fetal Bovine Serum; FDA, Food and Drugs Administration; NIR, near-infrared; NPs, nanoparticles; OCT, optimal cutting temperature; PBS, phosphate buffered saline; PDI, polydispersity index; Phalloidin-TRITC, Phalloidin–Tetramethylrhodamine B isothiocyanate; PLGA, Poly(D,L-lactide-co-glycolide) acid; PTT, photothermal therapy; PVA, poly(vinyl alcohol); SLN, sentinel lymph nodes; SLNB, sentinel lymph nodes biopsy; TEM, transmission electron microscope.

Acknowledgments

We acknowledge help from Dr. Mirjam Geibel at the Zeiss Microscopy Customer Center Europe, Carl Zeiss Microscopy GmbH in Oberkochen, Germany for imaging the NIR-797–loaded PLGA NPs in vitro samples. The graphical abstract was Created with BioRender.com.

Funding

This work was supported by a grant from the Ministry of Research and Innovation, CNCS-UEFISCDI, project number PN-III-P4-ID-PCCF-2016-0142, within PNCDI III and by the project Plasmon mediated biology: Exploitation of plasmonics to investigate and enhance biological processes and application to biomedical issues (acronym: BioPlasmonics) funded by European Union – NextgenerationEU and Romanian Government, under National Recovery and Resilience Plan for Romania, contract no760037/23.05.2023, cod PNRR-C9-I8-CF-199/28.11.2023, through the Romanian Ministry of Research, Innovation and Digitalization, within Component 9, Investment I8. Madalina Tudor is thankful for the Special Scholarship for Scientific Activity, grant awarded by STAR-UBB (Babes-Bolyai University), contract number 36617/25.11.2022.

Disclosure

The authors report no conflicts of interest in this work.

References

1. Sung H, Ferlay J, Siegel RL, et al. Global cancer statistics 2020: GLOBOCAN estimates of incidence and mortality worldwide for 36 cancers in 185 countries. *Ca a Cancer J Clin*. 2021;71(3):209–249. doi:10.3322/caac.21660
2. Cancer facts & figures 2022. 2022.
3. Clarke EL, Wade RG, Magee D, Newton-Bishop J, Treanor D. Image analysis of cutaneous melanoma histology: a systematic review and meta-analysis. *Sci Rep*. 2023;13(1):4774. doi:10.1038/s41598-023-31526-7
4. Nwafor JN, Torere BE, Agu E, et al. The role of biomarkers in the diagnosis and prognosis of different stages of melanoma. *Cureus*. 2023. 10.7759/cureus.38693
5. Valsecchi ME, Silbermins D, De Rosa N, Wong SL, Lyman GH. Lymphatic mapping and sentinel lymph node biopsy in patients with melanoma: a meta-analysis. *JCO*. 2011;29(11):1479–1487. doi:10.1200/JCO.2010.33.1884
6. Lese I, Constantinescu MA, Leckenby JI, et al. Transcutaneous sentinel lymph node detection in cutaneous melanoma with indocyanine green and near-infrared fluorescence: a diagnostic sensitivity study. *Medicine*. 2022;101(36):e30424. doi:10.1097/MD.0000000000030424
7. Zeng HC, Hu JL, Bai JW, Zhang GJ. Detection of sentinel lymph nodes with near-infrared imaging in malignancies. *Mol Imaging Biol*. 2019;21(2):219–227. doi:10.1007/s11307-018-1237-4
8. Zhang RR, Schroeder AB, Grudzinski JJ, et al. Beyond the margins: real-time detection of cancer using targeted fluorophores. *Nat Rev Clin Oncol*. 2017;14(6):347–364. doi:10.1038/nrclinonc.2016.212
9. Van Keulen S, Hom M, White H, Rosenthal EL, Baik FM. The evolution of fluorescence-guided surgery. *Mol Imaging Biol*. 2023;25(1):36–45. doi:10.1007/s11307-022-01772-8
10. Refaat A, Yap ML, Pietersz G, et al. In vivo fluorescence imaging: success in preclinical imaging paves the way for clinical applications. *J Nanobiotechnol*. 2022;20(1):450. doi:10.1186/s12951-022-01648-7
11. Mieog JSD, Achterberg FB, Zlitni A, et al. Fundamentals and developments in fluorescence-guided cancer surgery. *Nat Rev Clin Oncol*. 2022;19(1):9–22. doi:10.1038/s41571-021-00548-3
12. Austin E, Geisler AN, Nguyen J, et al. Visible light. Part I: properties and cutaneous effects of visible light. *J Am Acad Dermatol*. 2021;84(5):1219–1231. doi:10.1016/j.jaad.2021.02.048
13. Hernot S, Van Manen L, Debie P, Mieog JSD, Vahrmeijer AL. Latest developments in molecular tracers for fluorescence image-guided cancer surgery. *Lancet Oncol*. 2019;20(7):e354–e367. doi:10.1016/S1470-2045(19)30317-1
14. Dheyab MA, Aziz AA, Khaniabadi PM, et al. Gold nanoparticles-based photothermal therapy for breast cancer. *Photodiagn Photodyn Ther*. 2023;42:103312. doi:10.1016/j.pdpdt.2023.103312
15. Báez DF. Graphene-based nanomaterials for photothermal therapy in cancer treatment. *Pharmaceutics*. 2023;15(9):2286. doi:10.3390/pharmaceutics15092286
16. Duan S, Hu Y, Zhao Y, et al. Nanomaterials for photothermal cancer therapy. *RSC Adv*. 2023;13(21):14443–14460. doi:10.1039/D3RA02620E
17. Millard M, Bernhard Y, Canilho N, et al. Enhanced stability and photothermal efficiency of indocyanine green j-aggregates by nanoformulation with calix[4]arene for photothermal therapy of cancers. *Colloids Surf B*. 2023;230:113516. doi:10.1016/j.colsurfb.2023.113516
18. Li W, Ma T, He T, Li Y, Yin S. Cancer cell membrane–encapsulated biomimetic nanoparticles for tumor immuno-photothermal therapy. *Chem Eng J*. 2023;463:142495. doi:10.1016/j.cej.2023.142495
19. Tang K, Li X, Hu Y, et al. Recent advances in Prussian blue-based photothermal therapy in cancer treatment. *Biomater Sci*. 2023;11(13):4411–4429. doi:10.1039/D3BM00509G
20. Xiong Y, Rao Y, Hu J, Luo Z, Chen C. Nanoparticle-based photothermal therapy for breast cancer noninvasive treatment. *Adv. Mater.* 2023:2305140. doi:10.1002/adma.202305140
21. Gao G, Sun X, Liang G. Nanoagent-promoted mild-temperature photothermal therapy for cancer treatment. *Adv Funct Mater*. 2021;31(25):2100738. doi:10.1002/adfm.202100738
22. Ng KK, Zheng G. Molecular interactions in organic nanoparticles for phototheranostic applications. *Chem Rev*. 2015;115(19):11012–11042. doi:10.1021/acs.chemrev.5b00140
23. Payne M, Bossmann SH, Basel MT. Direct treatment versus indirect: thermo-ablative and mild hyperthermia effects. *WIREs Nanomed Nanobiotechnol*. 2020;12(5):e1638. doi:10.1002/wnan.1638
24. Borlan R, Focsan M, Maniu D, Astilean S. Interventional NIR fluorescence imaging of cancer: review on next generation of dye-loaded protein-based nanoparticles for real-time feedback during cancer surgery. *IJN*. 2021;16:2147–2171. doi:10.2147/IJN.S295234
25. Lafreniere AS, Shine JJ, Nicholas CR, Temple-Oberle CF. The use of indocyanine green and near-infrared fluorescence imaging to assist sentinel lymph node biopsy in cutaneous melanoma: a systematic review. *Eur J Surg Oncol*. 2021;47(5):935–941. doi:10.1016/j.ejso.2020.10.027
26. Wang J, Liao H, Ban J, et al. Multifunctional near-infrared dye IR-817 encapsulated in albumin nanoparticles for enhanced imaging and photothermal therapy in melanoma. *IJN*. 2023;18:4949–4967. doi:10.2147/IJN.S425013
27. Chen Z, Chen Y, Xu Y, et al. BODIPY-based multifunctional nanoparticles for dual mode imaging-guided tumor photothermal and photodynamic therapy. *ACS Appl Bio Mater*. 2023;6(9):3406–3413. doi:10.1021/acsabm.3c00083
28. Xue J, Zhu Y, Bai S, et al. Nanoparticles with rough surface improve the therapeutic effect of photothermal immunotherapy against melanoma. *Acta Pharmaceutica Sinica B*. 2022;12(6):2934–2949. doi:10.1016/j.apsb.2021.11.020
29. Alsaab HO, Alharbi FD, Alhibs AS, et al. PLGA-based nanomedicine: history of advancement and development in clinical applications of multiple diseases. *Pharmaceutics*. 2022;14(12):2728. doi:10.3390/pharmaceutics14122728
30. Khalin I, Severi C, Heimburger D, et al. Dynamic tracing using ultra-bright labeling and multi-photon microscopy identifies endothelial uptake of poloxamer 188 coated poly(lactic-co-glycolic acid) nano-carriers in vivo. *Nanomed Nanotechnol Biol Med*. 2022;40:102511. doi:10.1016/j.nano.2021.102511
31. Patel RH, Wadajkar AS, Patel NL, Kavuri VC, Nguyen KT, Liu H. Multifunctionality of indocyanine green-loaded biodegradable nanoparticles for enhanced optical imaging and hyperthermia intervention of cancer. *J Biomed Opt*. 2012;17(4):046003. doi:10.1117/1.JBO.17.4.046003
32. Elmowafy EM, Tiboni M, Soliman ME. Biocompatibility, biodegradation and biomedical applications of poly(lactic acid)/poly(lactic-co-glycolic acid) micro and nanoparticles. *J Pharm Investig*. 2019;49(4):347–380. doi:10.1007/s40005-019-00439-x

33. Ghasemi M, Liang S, Luu QM, Kempson I. The MTT assay: a method for error minimization and interpretation in measuring cytotoxicity and estimating cell viability. In: Friedrich O, Gilbert DF editors. *Cell Viability Assays: Methods and Protocols*. Springer US; 2023:15–33. doi:10.1007/978-1-0716-3052-5_2
34. Overwijk WW, Restifo NP. B16 as a mouse model for human melanoma. *CP Immunol*. 2000;39(1). doi:10.1002/0471142735.im2001s39
35. Zhirnik AS, Nikolskaya ED, Zhunina OA, et al. Evaluation of the uptake of PLGA-PEG nanoparticles by human cancer cells. *Nanotechnol Russia*. 2018;13(1–2):67–75. doi:10.1134/S1995078018010147
36. Kobayashi H, Watanabe R, Choyke PL. Improving Conventional Enhanced Permeability and Retention (EPR) Effects; What Is the appropriate target? *Theranostics*. 2014;4(1):81–89. doi:10.7150/thno.7193
37. Bertocchi F, Delledonne A, Vargas-Nadal G, Terenziani F, Painelli A, Sissa C. Aggregates of cyanine dyes: when molecular vibrations and electrostatic screening make the difference. *J Phys Chem C*. 2023;127(21):10185–10196. doi:10.1021/acs.jpcc.3c01253
38. Pan GY, Jia HR, Zhu YX, Wang RH, Wu FG, Chen Z. Dual channel activatable cyanine dye for mitochondrial imaging and mitochondria-targeted cancer theranostics. *ACS Biomater Sci Eng*. 2017;3(12):3596–3606. doi:10.1021/acsbiomaterials.7b00480
39. Borlan R, Focsan M, Perde-Schrepler M, et al. Antibody-functionalized theranostic protein nanoparticles for the synergistic deep red fluorescence imaging and multimodal therapy of ovarian cancer. *Biomater Sci*. 2021;9(18):6183–6202. doi:10.1039/D1BM01002F
40. Xiao Y, An F, Chen J, et al. The nanoassembly of an intrinsically cytotoxic near-infrared dye for multifunctionally synergistic theranostics. *Small*. 2019;15(38):1903121. doi:10.1002/smll.201903121
41. Ferrari De Andrade L. Methods to microscopically analyze melanoma tumors in mice. *J Histotechnol*. 2015;38(3):75–82. doi:10.1179/2046023615Y.0000000007
42. Guitera P, Li LXL, Scolyer RA, Menzies SW. Morphologic features of melanophages under in vivo reflectance confocal microscopy. *Arch Dermatol*. 2010;146(5). doi:10.1001/archdermatol.2009.388
43. Porcellato I, Sforna M, Lo Giudice A, et al. Tumor-associated macrophages in canine oral and cutaneous melanomas and melanocytomas: phenotypic and prognostic assessment. *Front Vet Sci*. 2022;9:878949. doi:10.3389/fvets.2022.878949
44. Mihm MC, Mulé JJ. Reflections on the histopathology of tumor-infiltrating lymphocytes in melanoma and the host immune response. *Cancer Immunol Res*. 2015;3(8):827–835. doi:10.1158/2326-6066.CIR-15-0143
45. Day CL, Lew RA, Mihm MC, et al. A multivariate analysis of prognostic factors for melanoma patients with lesions > 3.65 mm in thickness the importance of revealing alternative cox models*. *Ann Surg*. 1982;195(1):44–49. doi:10.1097/00000658-198201001-00007
46. Dąbrowska-Bouta B, Sulkowski G, Gewartowska M, Strużyńska L. Endoplasmic reticulum stress underlies nanosilver-induced neurotoxicity in immature rat brain. *IJMS*. 2022;23(21):13013. doi:10.3390/ijms232113013
47. Gomes LC, Benedetto GD, Scorrano L. During autophagy mitochondria elongate, are spared from degradation and sustain cell viability. *Nat Cell Biol*. 2011;13(5):589–598. doi:10.1038/ncb2220
48. Shubin AV, Demidyuk IV, Komissarov AA, Rafieva LM, Kostrov SV. Cytoplasmic vacuolization in cell death and survival. *Oncotarget*. 2016;7(34):55863–55889. doi:10.18632/oncotarget.10150

International Journal of Nanomedicine Dovepress

Publish your work in this journal

The International Journal of Nanomedicine is an international, peer-reviewed journal focusing on the application of nanotechnology in diagnostics, therapeutics, and drug delivery systems throughout the biomedical field. This journal is indexed on PubMed Central, MedLine, CAS, SciSearch®, Current Contents®/Clinical Medicine, Journal Citation Reports/Science Edition, EMBase, Scopus and the Elsevier Bibliographic databases. The manuscript management system is completely online and includes a very quick and fair peer-review system, which is all easy to use. Visit http://www.dovepress.com/testimonials.php to read real quotes from published authors.

Submit your manuscript here: https://www.dovepress.com/international-journal-of-nanomedicine-journal